# Internal Solitary Waves and Floating Bodies

**Samuel Hartharn-Evans**[a], **Magda Carr**[b], **Marek Stastna**[c]
a. Department of Geography & Environmental Sciences, Northumbria University, UK.
b. School of Mathematics, Statistics & Physics, Newcastle University, UK.
c. Department of Applied Mathematics, University of Waterloo, Canada.
Email: magda.carr@newcastle.ac.uk

## 1 Introduction

Internal Solitary Waves (ISWs) that form on internal density interfaces within the ocean are responsible for the horizontal transport and vertical mixing of heat, nutrients, and other water properties. The waves also induce flow that can cause stresses on and motion of floating surface bodies, such as sea ice (Carr et al. (2019)) and offshore wind infrastructure (Wang et al. (2018)). This study investigates ISW-surface body interactions. Using laboratory experiments, ISWs interacting with weighted floats of varying sizes are observed. It is shown that the motion of the floats can be modelled effectively by simply using the average velocity of the fluid under the float. It is found that when floats are small relative to the wavelength, they behave in the same manner as a fluid particle, but as floats become bigger relative to the wavelength, the maximum velocity they can attain decreases, as float-flow interaction time increases. This phenomenon is explained by the wave-induced flow as opposed to energy transfer arguments. By using this model with a large sample of theoretical waves from a Dubriel-Jacotin-Long (DJL) model (Dunphy et al. (2011)), the float motion is parameterised based on the float length and wave parameters.

## 2 Laboratory Study

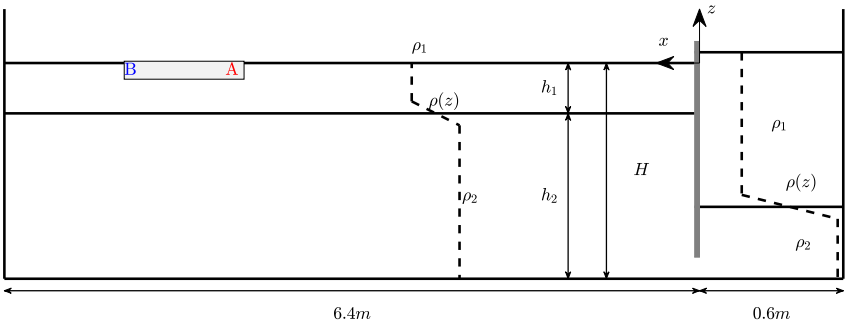


Figure 1: Schematic diagram of laboratory set-up, indicating the stratification type by the density profile, $\rho(z)$, and the location of an oblong floating body labelled with faces A and B.

The experiments were carried out at Newcastle University in a wave flume 7 m long, 0.4 m wide and 0.6 m high, described within a Cartesian coordinate system ($x$, $y$, $z$). The $x$ and $z$ directions denote the horizontal direction of wave propagation (from right to left) and vertical direction against gravity, respectively. A removable vertical gate, located at $x = 0$ separated the flume into two sections, a main section $x > 0$ and a wave generating section $x < 0$. Removal of the gate and subsequent buoyancy driven

flow adjustment result in the generation of an ISW of depression which propagates into the main section of the flume and interacts with the floating body placed downstream. The flow was visualised using neutrally buoyant light reflecting tracer particles and the velocity field measured via Particle Image Velocimetry (PIV).

# 3 Float Motion Model (FMM)

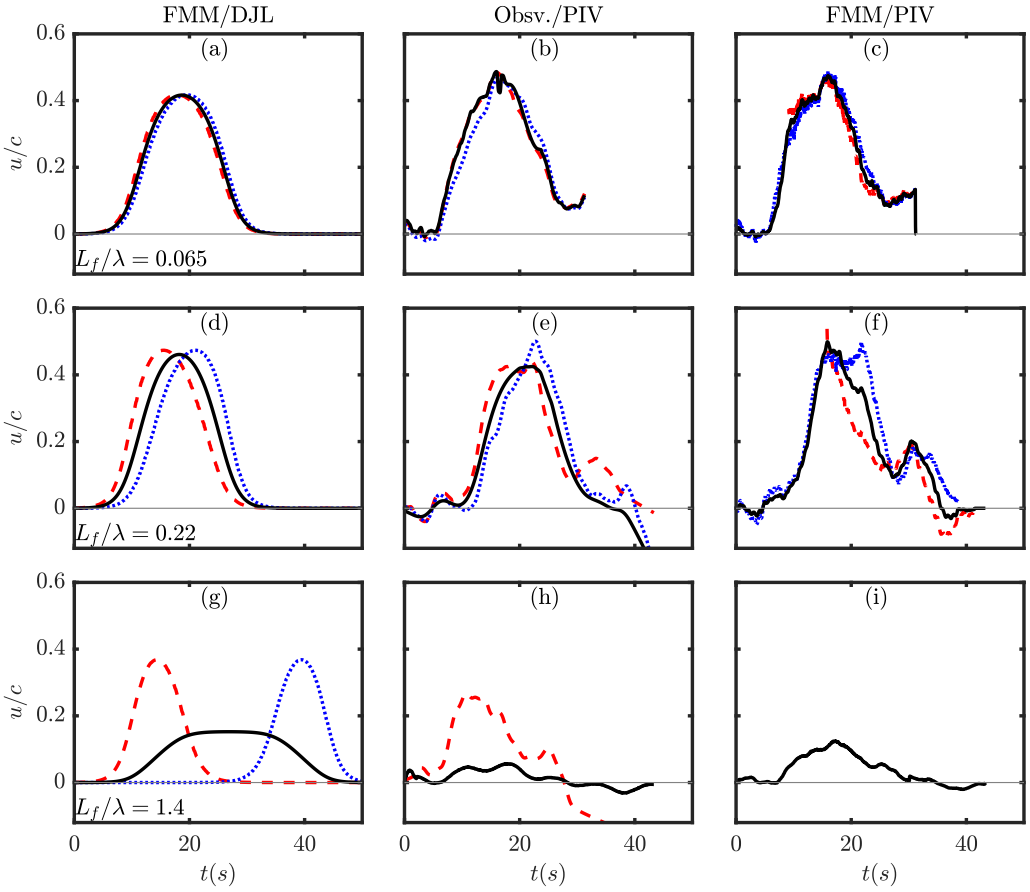


Figure 2: Time series of float velocity (black/solid) during the passage of an ISW for three floats of varying lengths (a-c representing $L_f = 0.1m$, d-f representing $L_f = 0.35m$ and g-i representing $L_f = 2.4m$), and the horizontal fluid velocity at points A (red/dashed) and B (blue/dotted) on the float. The left column (a, d, g) shows the FMM applied to DJL velocity data, the central column (b, e, h) shows the observed float motion, and the right column (c, f, i) showing the FMM applied to observed PIV velocities. All velocities are normalised by the ISW propagation speed, $c$.

The float motion model (FMM) routine solves the equation:

$$\frac{dx_f}{dt} = U(t) = \frac{\iint u(x_f(t), t)\, dx\, dy}{\iint dx\, dy},$$

where $x_f(t)$ is the horizontal position of the centre of the float at time, $t$, and $U$ is the horizontal velocity of the float, for a choice of two input horizontal velocity signals, $u = u_{DJL}$ or $u = u_{PIV}$ from the fully nonlinear DJL equation or PIV from the laboratory

experiments respectively. Figure 2 gives a comparison of the results. Excellent agreement between the FMM (either with DJL or PIV) and laboratory observations when the floating body is relatively small (panels (a)-(f)) is seen. Discrepancies become more apparent for larger float lengths (panels (g)-(i)). This is expected as it was observed that whilst small floats do not disrupt the flow patterns larger ones do. In particular, the wave-induced flow under larger floats forms a pair of counter-rotating vortices at each end of the float. The formation and evolution of these flow features arise as a result of boundary layer separation with the horizontal wave-induced flow relative to the float velocity. This reveals complex dynamics due to the non-stationary behaviour of both the float and flow. The relationship between float size, wave size and the motion of the

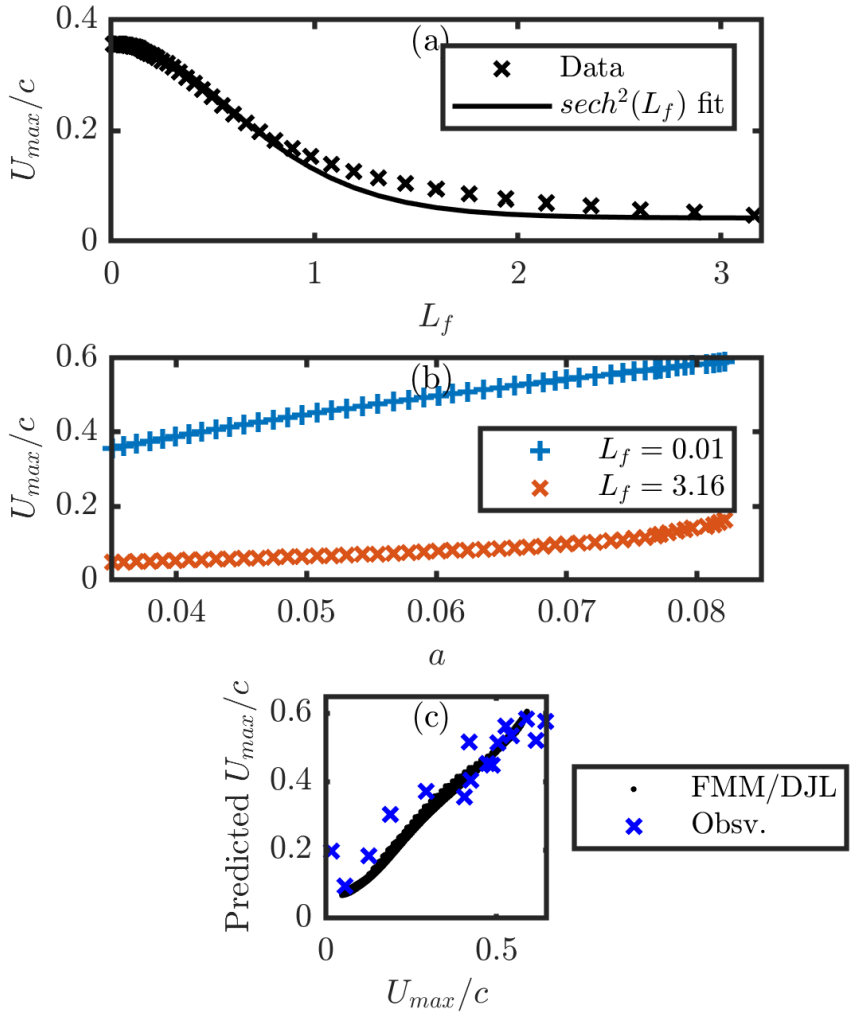


Figure 3: Indicative illustrations of the relationship between (a) float length, $L_f$, and maximum float speed, $U_{max}/c$, from FMM/DJL, (b) wave amplitude, $a$, and $U_{max}/c$, and (c) goodness of fit of equation (1) to observations for the FMM/DJL (black dots) and direct measurements from the laboratory experiments (blue x).

float can be explored using FMM/DJL. Figure 3 (a) shows the relationship between float length, $L_f$, and maximum float velocity, $U_{max}$, for a small ($a = 0.0351$ m) DJL wave. Figure 3 (a) shows that $U_{max}/c \propto sech^2(L_f)$, and maximum float speed decreases with increasing float length, this $sech^2$ relationship arising entirely empirically. The effect of increasing the wave amplitude, $a$, is to increase the maximum float speed, although the

effect is stronger for a very small float ($L_f = 0.1$ m, figure 3 b, blue dotted line) than for larger floats (red dashed line, figure 3 b). A parameterisation of the wave-induced float motion is captured by the following relationship:

$$\frac{U_{max}}{c} = \left(b_0 \frac{a}{H} + b_1\right)\left(sech^2\left(\frac{L_f}{b_2\lambda + b_3}\right) + b_4\right) \tag{1}$$

where $b_0 = 1.2458, b_1 = 0.1538, b_2 = 0.6681, b_3 = -0.1870$, and $b_4 = 0.2233$, are calculated empirically. The goodness of fit measure between this parameterisation and observations is $R^2 = 0.9969$ when ($n = 2940$) FMM/DJL solutions are used, and $R^2 = 0.8579$ when Obsv./PIV measures are utilised (figure 3 c).

**Acknowledgments**
This work has recently been accepted for publication, see Hartharn-Evans et al. (2023). We thank Dunphy et al. (2011) for their DJLES code used in this project, which is freely available at https://github454 .com/mdunphy/DJLES. Technical assistance in the Novak Laboratory at Newcastle University was provided by Jonathan Bell and Stuart Patterson and is gratefully acknowledged. This work was supported by the Natural Environment Research Council (NERC) funded ONE Planet Doctoral Training Partnership (S.H.E., grant number [NE/S007512/1]).

# References

Carr, M., Sutherland, P., Haase, A., Evers, K. U., Fer, I., Jensen, A., Kalisch, H., Berntsen, J., Parau, E., Thiem, O. & Davies, P. A. (2019), 'Laboratory Experiments on Internal Solitary Waves in Ice-Covered Waters', *Geophysical Research Letters* **46**(21), 12230–12238.

Dunphy, M., Subich, C. & Stastna, M. (2011), 'Spectral methods for internal waves: Indistinguishable density profiles and double-humped solitary waves', *Nonlinear Processes in Geophysics* **18**(3), 351–358.

Hartharn-Evans, S. G., Carr, M. & Stastna, M. (2023), 'Interaction between internal solitary waves and sea-ice', *Journal of Geophysical Research: Oceans.* (In press).

Wang, X., Zhou, J.-F., Wang, Z. & You, Y.-X. (2018), 'A numerical and experimental study of internal solitary wave loads on semi-submersible platforms', *Ocean Engineering* **150**, 298–308.